Università degli studi di Padova

DIPARTIMENTO DI FISICA ED ASTRONOMIA "GALILEO GALILEI"
Corso di Laurea in Fisica

MEASUREMENT OF THE SURFACE SUSCEPTIBILITY AND CONDUCTIVITY OF ATOMICALLY THIN MoS_2 AND WS_2 BY SPECTROSCOPIC ELLIPSOMETRY

Relatore:
Chiar.mo Prof.
Michele Merano

Correlatore:
Chiar.mo Prof.
Alessandro Martucci

Laureando:
Bagnarol Mirko
mat. 1096581

Anno Accademico 2016-2017

Per aspera sic itur ad astra

Ad Irene, Luciano, Alberta e Raffaele
Agli Ammiratori, agli Avengers, a Dirty Dancing
e a Romelu Lukaku per il sostegno in quest'ultimo anno fantastico

Contents

Chapter 1

Atomically thin transition metal dichalcogenides

1.1 Definition and properties

Transition metals dichalcogenide (TMD) monolayers are a group of bidimensional direct band gap semiconductors. They are composed by a layer of a transition metal, such as *Mo* and *W*, between two layers of a chalcogen, such as *S*, *Se* or *Te* [1]. Their structure is composed of an hexagonal plane of transition metal atoms placed between two hexagonal planes of chalcogen atoms in a trigonal prismatic arrangement with strong covalent in-plane bonds and weak van der Waals coupling between the individual planes [2]. TMDs show that their properties are significantly modified by changing the number of layers. In fact, in the monolayer limit, these materials have often superior electronic, optical, catalytic and mechanical properties compared to their three-dimensional counterparts. They have an intrinsic band gap in the visible which crosses over from an indirect gap in bulk to a direct gap when reduced to a single atomic layer. Moreover, the photocatalytic stability is significantly increased in the monolayer limit compared to any multiple layers making these materials interesting for optoelectronic applications and solar energy harvesting [3]. Furthermore, both the conduction and valence bands of monolayer TMDs have two degenerate energy valleys at the corners of the first Brillouin zone, which are essential to optically control the charge carriers in these valleys. These properties make possible a new class of integration in spintronics and valleytronics [4]. With such a broad potential application base, a comprehension of the optical properties of TMDs, and in particular of MoS_2, is going to elucidate their electronic band structure which is critical to electronic and optoelectronic device researchers.

1.1.1 Band gap crossover

The most important property of these new class of materials is the already mentioned transition from an indirect to a direct band gap in the passage from bulk to monolayer. We are now analyzing this fact showing the most important results deeply examined in [1] for MoS_2. The evolution of the optical properties and electronic structure of ultrathin MoS_2 crystals by changing layer number N from 1 to 6 is examined by using three complementary spectroscopic techniques: optical absorption, photoluminescence (PL) and photoconductivity. The combination of these spectroscopic methods allowed them to trace the evolution of both the indirect and direct band gaps of the material as a function of layer thickness N. By decreasing N, the experiments reveal a progressive confinement-induced shift in the indirect gap from the bulk value of ≈ 1.29 eV to over

$\approx$ 1.90 eV. The change in the indirect-gap energy was found to be significantly larger than that of the direct gap, which increased by only 0.1 eV. As a consequence of these different scaling properties, the MoS_2 crystals exhibit a crossover from an indirect to a direct gap semiconductor in the monolayer limit. In addition to the signatures of this effect in the absorption and photoconductivity spectra, the PL quantum yield showed a dramatic enhancement in going from the dark, indirect-gap bulk crystal to the bright, direct-gap monolayer, which stresses the passage from phonon to photon emission by electrons while crossing the band gap. For some suspended samples, they observed an increase of the PL quantum yeld by more than a factor of 10^4 for the monolayer compared with the bulk crystal. Now we are summing up a possible proof of this shift. In this simplified treatment of the spectral dependence of the photoconductivity, they neglected both any excitonic effect and the variation of matrix elements with energy. The absorbance $A(\hbar\omega)$ at photon energy $\hbar\omega$ near a direct band edge of energy E_g is then determined by the joint density of states. For a 2D material like MoS_2, this is described by the step function $\Theta(\hbar\omega - E_g)$. After including a phenomenological broadening of 30 meV to account for finite temperature and scattering rates, they found that the photoconductivity spectrum of the monolayer samples can be fit well to this simple model. This indicates that monolayer MoS_2 is indeed a direct-gap material. On the other hand, the photoconductivity spectrum for bilayer MoS_2 cannot be described by the step-function response. It is needed to include the effect of an indirect transition. Near an indirect band edge, the corresponding absorbance can be represented by expression

$$A(\hbar\Omega) \propto \sum_{\alpha} \left[\frac{\hbar\omega - \hbar\Omega_\alpha - E'_g}{1 - e^{\frac{-\hbar\Omega_\alpha}{kT}}} + \frac{\hbar\omega + \hbar\Omega_\alpha - E'_g}{e^{\frac{\hbar\Omega_\alpha}{kT}} - 1} \right] \propto \hbar\omega - E'_g \tag{1.1}$$

Here E'_g and $\hbar\Omega_\alpha$ denote, respectively, the indirect-gap energy and that of the αth phonon mode, and kT is the thermal energy. By taking this term into account, the experimental bilayer MoS_2 spectrum can be fit well by an indirect transition at 1.6 eV, combined with a direct transition at 1.88 eV This property causes monolayer TMDs to be more attractive than graphene for future transistors and logic circuit applications where a high on/off current ratio is required.

1.2 Production

In this section we are presenting the two most used production techniques for monolayer TMDs, also mentioning two other recent alternatives.

1.2.1 Exfoliation

The first and simplest production method is mechanical exfoliation, which consists of taking away some layers from bulk TMD using adhesive tape and depositing it in a silicon or glass substrate. To obtain a monolayer sample several intermediate exfoliation steps are required [5]. Each sample must be characterised because it can be made by one to many layers, and has a random shape. Another class of exfoliation method is through a chemical approach with solvent-based exfoliation. For instance, in [6] is presented an exfoliation method using TMD dispersion in water by elevating the temperature of the sonication bath and introducing energy in the system through dissipation of sonic waves.

1.2.2 CVD

An alternative and more elaborated technique to obtain TMD monolayers is by *Chemical Vapor Deposition* (CVD). The instrumentation consists of a quartz tube furnace with a hot zone at a working temperature of $\approx$ 1100 K, which hosts in the middle the transition metal oxide (such as molybdenum trioxide, MoO_3) over the desired substrate in an aluminia boat and the chalcogen powder in another aluminia boat, usually placed upstream of the first boat. After some preliminary procedures to eliminate residual water and physisorbed contaminants in the tube and in the substrate, the quartz tube is filled with a noble gas, such as argon (Ar), at a pressure of $\approx$ 53000 Pa and heated to the high worling temperature. Both the transition metal and chalcogen are carried by the noble gas and chemically react forming the desired TMD and another fizzy product. After $\approx$ 20 min, the tube is slowly cooled down at room temperature and the TMD monolayer is formed [7]. The CVD process guarantees a high quality final product, even if it demands an high technological instrumentation and an elaborated process. The TMD monolayer produced can, however, present some inpurities. Moreover, this technique can produce both single crystal and policrystalline samples. A single crystal area can reach 100 μm^2, while policrystalline samples are much wider, up to $\approx$ 1 cm^2, but present several border conditions, one at each single crystal shape. In [8] is presented a CVD technique to obtain large area single crystal WS_2 samples, which reach $\approx 0.014 mm^2$

1.2.3 Innovative techiniques

Laser thinning

One single sample obtained via mechanical exfoliation may be composed by different flakes, each one with a different layer number and random shape. To obtain a precise-shaped TMD monolayer it is possible to scan the desired area and to thin the multilayer flakes by inducing sublimation with an high power laser with a certain setup, such as a scanning laser from a confocal Raman microscope. The sublimation of the upper layers occurs because of the heat induced by light absorption, and the bottom layer is immune to sublimation because it is in intimate contact with the substrate which acts as a heat sink, thus it need a much higher laser power to be separated and to sublimate. Using the Raman microscope experimental setup it is possible to reach a production of $\approx 8 \frac{\mu m^2}{min}$. However this method produces samples about three times rougher than pristine TMD because of unremoved TMD traces on the surface [9].

Thermal annealing

Samples obtained via mechanical exfoliation can vary from more than five-layer to monolayer. To thin layer by layer the sample, after having determinated the layer number, it is possible to set the sample along with the silicon substrate in a quartz tube and induce sublimation of the TMD. Using argon (Ar) gas at 500 K and 1333.22 Pa can guarantee a thinning rate of $\approx 1 \frac{\text{Layer lost}}{h}$. However this method, even if economic, causes the TMD's surface to shrink. This is because the sublimation occurs both perpendiculary and in parallel to the material surface [10].

Chapter 2

Optical models for 2D materials

The study of monolayer materials began in 2004 with the discovery of graphene by A. Gejm and K. Novoselov. Since then the monolayer materials have been studied to understand their physical properties and, in particular, their electromagnetic properties. The model used to describe the interactions between an electromagnetic wave and graphene or monolayer TMDs has been initially the slab model, the model of propagation, reflection and trasmission of a classical electromagnetic wave through dielectric or conducting media [11], [12]. However there is also an alternative model, recently developed [13], which doesn't think of monolayer materials as an ultrathin strate of dielectric media but as a conducting plane which interacts only through opportune boundary conditions for the electric and magnetic field in the reflection and trasmission between the two media separated by the monolayer film. It is called the *surface current* model. In [14] it is showed that the surface current model fits better the graphene experimental data than the slab model used in the analysis. In [15] the authors derive the electric properties of several TMDs using the slab model and propose two relations that should make the models equivalent. In this work we are analyzing two of these TMDs, MoS_2 and WS_2, with both models to find out whether they are equivalent or not. In this chapter we are considering the two optical models mentioned.

2.1 Slab model

Let us consider a stratified medium, with electric and magnetic permittivity being respectively $\varepsilon = \varepsilon(z)$ and $\mu = \mu(z)$, calling $\hat{z}$ the axis perpendicular to the medium. Let us consider an incident plane electromagnetic wave which is linearly polarized such as its electric vector $\vec{E}$ is perpendicular to the plane of incidence, and let us denote as $\hat{x}$ that direction. Let also the wave be e^{iwt} time dependant. In this special case, the Maxwell's equations (in Lorentz-Heaviside units) are reduced to six scalar equations:

$$\begin{aligned} \frac{\partial H_z}{\partial y} - \frac{\partial H_y}{\partial z} + \frac{i\varepsilon\omega}{c} E_x = 0 \qquad & \qquad \frac{i\omega\mu}{c} H_x = 0 \\ \frac{\partial H_x}{\partial z} - \frac{\partial H_z}{\partial x} = 0 \qquad & \qquad \frac{\partial E_x}{\partial z} - \frac{i\omega\mu}{c} H_y = 0 \\ \frac{\partial H_y}{\partial x} - \frac{\partial H_x}{\partial y} = 0 \qquad & \qquad \frac{\partial E_x}{\partial y} + \frac{i\omega\mu}{c} H_z = 0 \end{aligned} \tag{2.1}$$

It is possible now to eliminate H_y and H_z and obtain a differential equation:

$$\frac{\partial^2 E_x}{\partial y^2} + \frac{\partial^2 E_x}{\partial z^2} + n^2 k_0^2 E_x = \frac{\mathrm{d} \ln \mu}{\mathrm{d}z} \frac{\partial E_x}{\partial z} \tag{2.2}$$

with $n^2 = \varepsilon\mu$ and $k_0 = \frac{2\pi}{\lambda_0}$. The method to solve this equation is beyond the purpose of this work, and we do not present it. It is fully described in [16] and we only summarize the most significant results to derive the *reflectivity* R and *trasmissivity* T.
Imposing the solution of equation 2.2 to be $E_x = Y(y)U(z)$, solving immediatly the y-related part of the equation obtaining $Y(y) = Ae^{ik_0\alpha y}$, A being a generic constant and with $\alpha = n\sin\theta$, and finally imposing $E_x = U(z)e^{i(k_0\alpha y - \omega t)}$ and $H_y = V(z)e^{i(k_0\alpha y - \omega t)}$, it is possible to write a system of two equations:

$$\begin{cases} \frac{\mathrm{d}^2U}{\mathrm{d}z^2} - \frac{\mathrm{d}\ \ln\ \mu}{\mathrm{d}z}\frac{\partial U}{\partial z} + k_0^2(n^2 - \alpha^2)U = 0 \\ \frac{\mathrm{d}^2V}{\mathrm{d}z^2} - \frac{\mathrm{d}\ \ln\ \left(\varepsilon - \frac{\alpha^2}{\mu}\right)}{\mathrm{d}z}\frac{\partial V}{\partial z} + k_0^2(n^2 - \alpha^2)V = 0 \end{cases} \tag{2.3}$$

The solutions of the system $U(z)$ and $V(z)$, deriving from two simultaneous equations, can be expressed as linear combination of two particolar solutions U_1, U_2 and V_1, V_2, which are not completely arbitrary but must satisfy some specific conditions. From these conditions the most convenient choice is

$$\begin{cases} U_1 &= f(z) \\ U_2 &= F(z) \end{cases} \qquad \begin{cases} V_1 &= g(z) \\ V_2 &= G(z) \end{cases} \tag{2.4}$$

such that $f(0) = G(0) = 0$ and $F(0) = g(0) = 1$. Supposing to have initial conditions $U(0) = U_0$ and $V(0) = V_0$, it is possible to put the solutions in the reversed matrix form $\boldsymbol{Q_0} = \boldsymbol{M}\ \boldsymbol{Q}$, where

$$\boldsymbol{M} = \begin{pmatrix} g(z) & -f(z) \\ -G(z) & F(z) \end{pmatrix} \tag{2.5}$$

We also note that $|\boldsymbol{M}| = 1$. Equation 2.5 means that to determinate the propagation of a plane monochromatic wave through a stratified medium, the medium only needs to be specified by a characteristic two by two unimodular matrix $\mathbf{M}$. For this reason $\mathbf{M}$ is called the *characteristic matrix* of the stratified medium.
Shall we now derive the general expressions for the *reflection* and *trasmission coefficients* r and t in the case of a dielectric film. Let us denote *I, R* and *T* the electric field amplitudes of the incident, reflected and transmitted wave, $\varepsilon_{1,2,3}$ and $\mu_{1,2,3}$ the electric and magnetic permeability of the first, middle and last materials and θ_i and θ_t the incident and transmittend angles. We must impose the continuity of the tangential components of $\vec{E}$ and $\vec{H}$ across the two boundaries of the stratified medium. This means that

$$\vec{H} = \sqrt{\frac{\varepsilon}{\mu}}\hat{s} \times \vec{E} \tag{2.6}$$

which gives the following relations for U and V:

$$\begin{cases} U_0 &= I + R \\ V_0 &= p_1(I - R) \end{cases} \qquad \begin{cases} U(\bar{z}) &= T \\ V(\bar{z}) &= p_3 T \end{cases} \tag{2.7}$$

with $\bar{z}$ being the depth where the film ends and the transmitted wave enters definetely in the third material. As *U, V,* U_0 and V_0 are bound by the relation $\boldsymbol{Q_0} = \boldsymbol{M}\ \boldsymbol{Q}$, detoning as $\bar{m}_{ij}$ the element at row i and column j of $\boldsymbol{M(\bar{z})}$, we have

$$\begin{cases} (\bar{m}_{11} + \bar{m}_{12}p_3)T &= I + R \\ (\bar{m}_{21} + \bar{m}_{22}p_3) &= p_1(I - R) \end{cases} \tag{2.8}$$

and finallt get

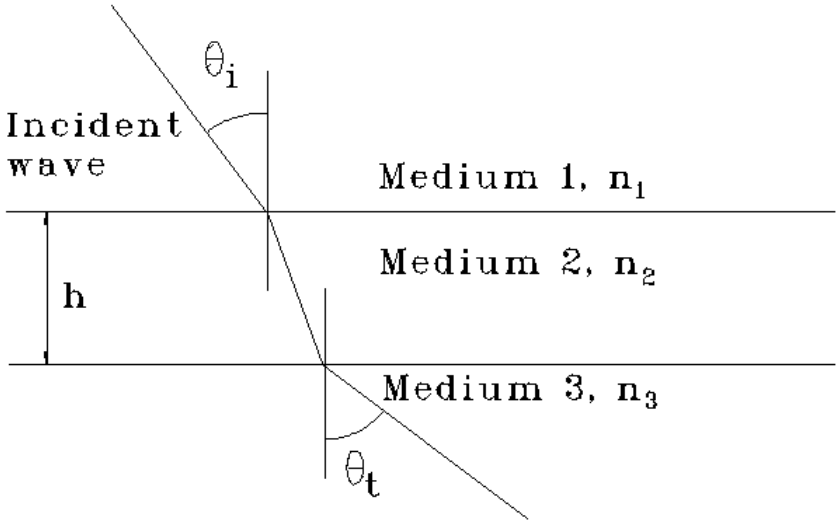

Figure 2.1: Scheme of the homogeneous dielectric film

$$r = \frac{R}{I} = \frac{(\bar{m}_{11} + \bar{m}_{12}p_3)p_1 - (\bar{m}_{21} + \bar{m}_{22}p_3)}{(\bar{m}_{11} + \bar{m}_{12}p_3)p_1 + (\bar{m}_{21} + \bar{m}_{22}p_3)} \quad t = \frac{T}{I} = \frac{2p_1}{(\bar{m}_{11} + \bar{m}_{12}p_3)p_1 + (\bar{m}_{21} + \bar{m}_{22}p_3)} \tag{2.9}$$

To get the *reflectivity* R and *transimissivity* T it is sufficient to calculate

$$R = |r|^2 \qquad T = \frac{p_3}{p_1}|t|^2 \tag{2.10}$$

Let us now turn our attention to an homogeneous dielectric film, which has ε, μ and $n = \sqrt{\varepsilon\mu}$ constants. Applying the equations 2.3 to this special case and denoting $p = \sqrt{\frac{\varepsilon}{\mu}}\cos\theta_i$, we obtain

$$\boldsymbol{M} = \begin{pmatrix} \cos(k_0 n z\cos\theta) & -\frac{i}{p}\sin(k_0 n z\cos\theta) \\ -ip\sin(k_0 n z\cos\theta) & \cos(k_0 n z\cos\theta) \end{pmatrix} \tag{2.11}$$

Let us also assume the film of thickness h to be located between two homogeneous media and all three media to be nonmagnetic, therefore with μ=1. We denote the three media and their refractive index as in picture 2.1. Appling the characteristic matrix in eq 2.11 we obtain:

$$m'_{11} = m'_{22} = \cos\beta \qquad m'_{12} = -\frac{i\sin\beta}{p_2} \qquad m'_{21} = -ip_2\sin\beta \tag{2.12}$$

with $\beta = \frac{2\pi}{\lambda}n_2 h\cos\theta$ and $p_i = n_i\cos\theta_i$. Remembering that the *Fresnel coefficiens* for two homogeneous materials 1 and 2 are:

$$r^s_{12} = \frac{n_1\cos\theta_1 - n_2\cos\theta_2}{n_1\cos\theta_1 + n_2\cos\theta_2} \qquad r^p_{12} = \frac{n_2\cos\theta_1 - n_1\cos\theta_2}{n_2\cos\theta_1 + n_1\cos\theta_2}$$
$$t^s_{12} = \frac{2n_1\cos\theta_1}{n_1\cos\theta_1 + n_2\cos\theta_2} \qquad t^p_{12} = \frac{2n_1\cos\theta_1}{n_2\cos\theta_1 + n_1\cos\theta_2} \tag{2.13}$$

having s for the normal component and p for the parallel component to the plane of incidence, with analogous expressions for $r_{23}^{s,p}$ and $t_{23}^{s,p}$, we finally obtain: [16]

$$r_{123} = \frac{r_{12} + r_{23}e^{2i\beta}}{1 + r_{12}r_{23}e^{2i\beta}} \qquad t_{123} = \frac{t_{12}t_{23}e^{2i\beta}}{1 + r_{12}r_{23}e^{2i\beta}} \tag{2.14}$$

using for all the *Fresnel coefficiens* the same s or p form. The reflectivity and trasmissivity are consequently given by:

$$R = |r|^2 = \frac{r_{12}^2 + r_{23}^2 + 2r_{12}r_{23}\cos 2\beta}{1 + r_{12}^2 r_{23}^2 + 2r_{12}r_{23}\cos 2\beta} \tag{2.15}$$

$$T = \frac{p_3}{p_1}|t|s^2 = \frac{n_3\cos\theta_3}{n_1\cos\theta_1}\frac{t_{12}^2 t_{23}^2}{1 + r_{12}^2 r_{23}^2 + 2r_{12}r_{23}\cos 2\beta} \tag{2.16}$$

We have, as expected, $R + T = 1$. We also define *Absorbance* the quantity

$$A = -\log_{10} T \tag{2.17}$$

2.1.1 χ and σ from slab model

We end this section mentioning the attenuation through a medium of significant thickness h, which is described by the *extinction coefficient* k. The wave description is identical to ideal, non-attenuating materials but redefining the refractive index $n = n_{ideal} - \mathrm{i}k$. However, considering a nonmagnetic material with μ=1, we have $n = \sqrt{\varepsilon}$. This means that ε is a complex number, composed by a real part ε_1 and an imaginary part ε_2 defined such that $n = \sqrt{\varepsilon} = \sqrt{\varepsilon_1 - \mathrm{i}\varepsilon_2}$. In [15] Heinz et al. state that from ε_1 and ε_2 it is possible to derive the electric susceptibility χ and conductivity σ through two important relations, such that

$$\chi = (\varepsilon_1 - 1)h \qquad \sigma = \frac{2\pi\varepsilon_2\varepsilon_0 ch}{\lambda} \tag{2.18}$$

with c the speed of light in vacuum. In presence of a monolayer material of known thickness, by finding out its refractive index n and thus ε_1 and ε_2, it is possible to switch between this classical model and the surface current model. However, the equivalence of the models is based on the truthfullness of equations 2.18 which is not proved, and must be verified or denied.

2.2 Surface current model

Let us consider a flat 2D crystal, composed of N atoms per cm^2, with an atomic polarizability α. If we apply an electric field in the plane of the crystal a macroscopic dipole moment arises and it is possible to define a density of polarisation $\vec{P}$. If the electric field is applied orthogonally to the 2D crystal, no effective macroscopic polarization is created. Indeed, to have a macroscopic polarization, the microscopic dipoles need to be aligned, to generate a macroscopic separation of charges. Let us also suppose that the 2D crystal is isotropic in its own plane. This hypothesis is realistic beacause of MoS_2's and WS_2's simmetric in-plane structure, which doesn't show any favourite axis. Let us also assume also that $\vec{P} = \varepsilon_0\chi\vec{E}$ where ε_0 is the vacuum permittivity and χ is the electric susceptibility. Wherever the polarization in matter changes with time there is an electric

current $\vec{J}_p$, a genuine motion of charges. The connection between rate of change of polarization and current density is $\vec{J}_p = \frac{\partial \vec{P}}{\partial t}$. It is important to note that in passing from a bulk to a 2D crystal the dimensions of $\vec{P}$ vary from $\frac{\mathrm{C}}{\mathrm{m}^2}$ to $\frac{\mathrm{C}}{\mathrm{m}}$, the dimensions of χ pass from a pure number to meters and $\vec{J}_p$ becomes $\frac{\mathrm{A}}{\mathrm{m}}$.
Let us first suppose that a horizontal 2D crystal is suspended in vacuum and that a plane wave with e^{iwt} time dependance falls onto it, thus having the refractive indexes $n_1 = n_2 = 1$. The relation between the electric field $\vec{E}$ and the magnetic field $\vec{H}$ in the incident, reflected and transmitted waves is $Z_0\vec{H} = \hat{s} \times \vec{E}$ where $\hat{s}$ is the Poynting versor and Z_0 is the impedance of vacuum. The boundary conditions are $\hat{z} \times (\vec{E_2} - \vec{E_1}) = 0$ and $\hat{z} \times (\vec{H_2} - \vec{H_1}) = \vec{J_p}$ where $\hat{z}$ is the versor along the vertical z axis. Thus we have tree conditions for s polarisation (on the left) and tree for p polarisation (on the right):

$$\begin{aligned} E_{x,i} + E_{x,r} &= E_{x,t} & \qquad E_{y,i} + E_{y,r} &= E_{y,t} \\ E_{x,i} + E_{x,r} &= \frac{P_x}{\varepsilon_0 \chi} & \qquad E_{y,i} - E_{y,r} &= \frac{P_y}{\varepsilon_0 \chi} \\ H_{x,i} - H_{x,r} &= H_{x,t} + i\omega P_y & \qquad H_{y,i} + H_{y,r} &= H_{y,t} + i\omega P_x \end{aligned} \tag{2.19}$$

where *i, r* and *t* subscripts stand for *incident, reflected* and *transmitted*. Defining $r^s = \frac{E_r}{E_p}$, $t^s = \frac{E_t}{E_p}$ and $r^p = \frac{H_r}{H_p}$, $t^p = \frac{H_t}{H_p}$ as the reflection and the transmission coefficients, we have:

$$r^s = -\frac{ik\chi}{ik\chi + 2\cos\theta_i} \qquad r^p = \frac{ik\chi\cos\theta_i}{ik\chi\cos\theta_i + 2} \tag{2.20}$$

and $t^s = r^s + 1$, $t^p = 1 - r^p$, with θ_i being the angle of incidence. In this special case, the reflectivity is $R^{s,p} = |r^{2s,p}|$, the transmissivity is $T^{s,p} = |t^{2s,p}|$, and their sum $R^{s,p} + T^{s,p} = 1$ shows that there is no absorption.
Shall we now consider physical conducting media and not void. We must apply the Ohm's law $\vec{J} = \sigma\vec{E}$. We assume again that $\vec{J}$ is null or negligible in a direction orthogonal to the crystal plane, and in-plane isotropy. The boundary conditions for $\vec{H}$ becomes now $\hat{z} \times (\vec{H_2} - \vec{H_1}) = \vec{J_p} + \vec{J}$. We also add to equation 2.19 two other conditions becoming from Ohm's law, the former for s polarisation and the latter for p polarisation:

$$E_{x,i} + E_{x,r} = \frac{J_x}{\sigma} \qquad E_{y,i} - E_{y,r} = \frac{J_y}{\sigma} \tag{2.21}$$

And consequently we obtain:

$$r^s = -\frac{ik\chi + Z_0\sigma}{ik\chi + Z_0\sigma + 2\cos\theta_i} \qquad r^p = \frac{(ik\chi + Z_0\sigma)\cos\theta_i}{(ik\chi + Z_0\sigma)\cos\theta_i + 2} \tag{2.22}$$

and having again and $t^s = r^s + 1$, $t^p = 1 - r^p$. As for a bulk material, conductivity is connected with the transformation of part of the electromagnetic energy into heat. In fact:

$$T^{s,p} + R^{s,p} = 1 - \frac{4\sigma Z_0}{4 + 4\sigma Z_0 + \sigma^2 Z_0^2 + k^2\chi^2} \approx 1 - \sigma Z_0 \tag{2.23}$$

Finally we are able to consider the reflection and the transmission coefficient for the case of a 2D crystal at the interface of two different bulk media with refractive indexes n_1

and n_2. The only difference is the relation between $\vec{E}$ and $\vec{H}$ in the incident, reflected and transmitted waves:

$$\frac{Z_0}{n_1}\vec{H}_{i,r} = \hat{z} \times \vec{E}_{i,r} \qquad \frac{Z_0}{n_2}\vec{H}_t = \hat{z} \times \vec{E}_t \tag{2.24}$$

We at last obtain:

$$r^s = \frac{n_1 \cos\theta_i - n_2 \cos\theta_t - ik\chi - \sigma Z_0}{n_1 \cos\theta_i + n_2 \cos\theta_t + ik\chi + \sigma Z_0} \quad r^p = \frac{n_2 \cos\theta_i - n_1 \cos\theta_t + (ik\chi + \sigma Z_0)\cos\theta_i \cos\theta_t}{n_2 \cos\theta_i + n_1 \cos\theta_t + (ik\chi + \sigma Z_0)\cos\theta_i \cos\theta_t} \tag{2.25}$$

having consequentially [14] $t^s = r^s + 1$ and $t^p = r^p \frac{n_2 \cos\theta_i}{n_1 \cos\theta_t}$

Chapter 3

Ellipsometry

Let us consider a classical electromagnetic wave E_1 on air inciding with an angle $\theta \neq 0$ against a reflecting material, and E_2 the reflected wave. Let us denote δ_1 E_1's phase difference between the parallel and perpendicular components to the plane of incidence and δ_2 the same phase difference between the analogous components of E_2. Let us call Δ the angle defined as

$$\Delta = \delta_1 - \delta_2. \tag{3.1}$$

Thus Δ is the phase difference upon reflection and can vary from 0 to 360°.
Moreover, the amplitude of both perpendicular and parallel components may change upon reflection. Because of this, given from any optical model $|r^p|$ and $|r^s|$, the ratios of the reflected wave amplitude to the incoming wave amplitude respectively for the parallel and perpendicular components, we define the angle Ψ as

$$\tan \Psi = \frac{|r^p|}{|r^s|} \tag{3.2}$$

The value of Ψ can vary from 0 to 90°.
Now let us define the quantity ρ as the complex ratio of the total reflection coefficients, that is

$$\rho = \frac{r^p}{r^s}. \tag{3.3}$$

Then the *Foundamental Equation of Ellipsometry* follows from ρ's definition, and is

$$\rho = \tan \Psi e^{i\Delta} \tag{3.4}$$

with i being the immaginary unit. From equations 3.4 and 3.2 we derive a second definition of Δ [17]

$$\Delta = \arg \frac{r^p}{r^s}. \tag{3.5}$$

By performing ellipsometry measurements we get experimental values of Ψ and Δ, as schematised in picture 3.2. We used the VASE ellipsometer made by *J. A. Woollam, NE, USA*, kept in the *Indutrial Engineering Department* in *via Marzolo 9, Padova (PD)*. All measurements were made by prof. Alessandro Martucci always using the same ellipsometer shown in picture 3.1.

(a) From back (b) In profile

Figure 3.1: Pictures of the VASE ellipsometer

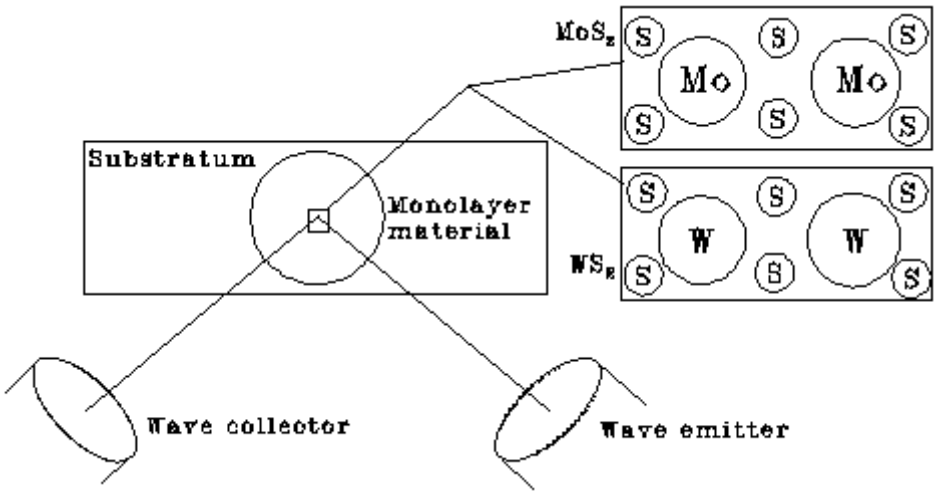

Figure 3.2: Scheme of the ellipsometer

Chapter 4

Measurements and data analysis

We obtained from different sources five samples of bidimensional material on subtrate, divided in two specimen of WS_2 and three specimen of MoS_2. They are:

- Sample 1 and 2 of WS_2 from IIT (Italian Institute of Technology) section of Pisa, prepared by Camilla Coletti's team
- Sample 1, 2 and 3 of MoS_2 from King Abdullah University of Science and Technology

All five spicemens were prepared using CVD technique. They all are policrystalline with area between 0.5 and 1 cm^2.

4.1 Substrate characterisation

We obtained ellipsometry measurements for each single monolayer material substrate, reported in figures 4.1 (b – d) and 4.2. Both samples of WS_2 and samples 1 and 2 of MoS_2 are on sapphire, while the last sample of MoS_2 is on soda-lime glass. As our substrates are of limited thickness with a rough end rather than endless, we obtained Ψ at each different angle correcting the recfractive index n, given by the Sellmeier formula, with an opportune addendum c_α to best fit experimental data.

4.1.1 Soda-lime glass

We considered three strata, the first topless and the last bottomless both made of air with $n_{air} \approx 1.00028$, and the middle one of thickness $h = 1$ mm made of soda-lime glass with the refractive index given by the *Sellmeier* formula [18]:

$$n_{BK7}(\lambda) = \sqrt{1 + \frac{1.03961212\lambda^2}{\lambda^2 - 0.00600069867} + \frac{0.231792344\lambda^2}{\lambda^2 - 0.0200179144} + \frac{1.01046945\lambda^2}{\lambda^2 - 103.560653}} \quad (4.1)$$

This formula needs λ to be in nm. We used n_{BK7} in place of $n_{Soda-lime}$ because they are experminetally equivalent in the λ range considered.
We then had the absorbance, defined in equation 2.17, from ellipsometry measurements at normal incidence and used it to derive the absorption coefficient k by the *Mathematica* algorithm `FindRoot`. At this point we interpolated the experimentals point dividing the λ spectrum in three intervals: exponential, linear and parabolic. We didn't impose any

boundary condition (such as logaritmical derivative equality), thus having completely free parameters. We have:

$$k(\lambda) = \begin{cases} e^{l-h\lambda} & if\ 300nm \leq \lambda < 336.1nm \\ q - m\lambda & if\ 336.1nm \leq \lambda < 356.7nm \\ a\lambda^2 + b\lambda + c & if\ 356.7nm \leq \lambda \leq 900nm \end{cases} \tag{4.2}$$

where the parameters have values $l = 5.4 \pm 1$, $h = 0.0552 \pm 0.0003\ nm^{-1}$, $q = (1.85 \pm 0.09)10^{-5}$, $m = (5.0 \pm 0.3)10^{-8}\ nm^{-1}$, $a = (4.6 \pm 0.2)10^{-12}\ nm^{-2}$, $b = (5.4 \pm 0.3)10^{-9}\ nm^{-1}$, $c = (2.34 \pm 0.07)10^{-6}$. Thus we put $n_{Soda-lime}(\lambda) = n_{BK7}^{Sellmeier}(\lambda) - i\,k(\lambda) + c_\alpha$ and varied c_α to best fit the experimental data of Ψ, calculating the theorical Ψ using equation 3.2, r^s and r^p being respectively r_{12}^s and r_{12}^p of equation 2.13. We show the results in the next table:

c_{35}	-0.012
c_{50}	0.002
c_{65}	0

We did not consider Δ as it is expected to be exactly 180° and difference between the theorical value and the measure is lower than the experimental error, which is between 2° and 3°.

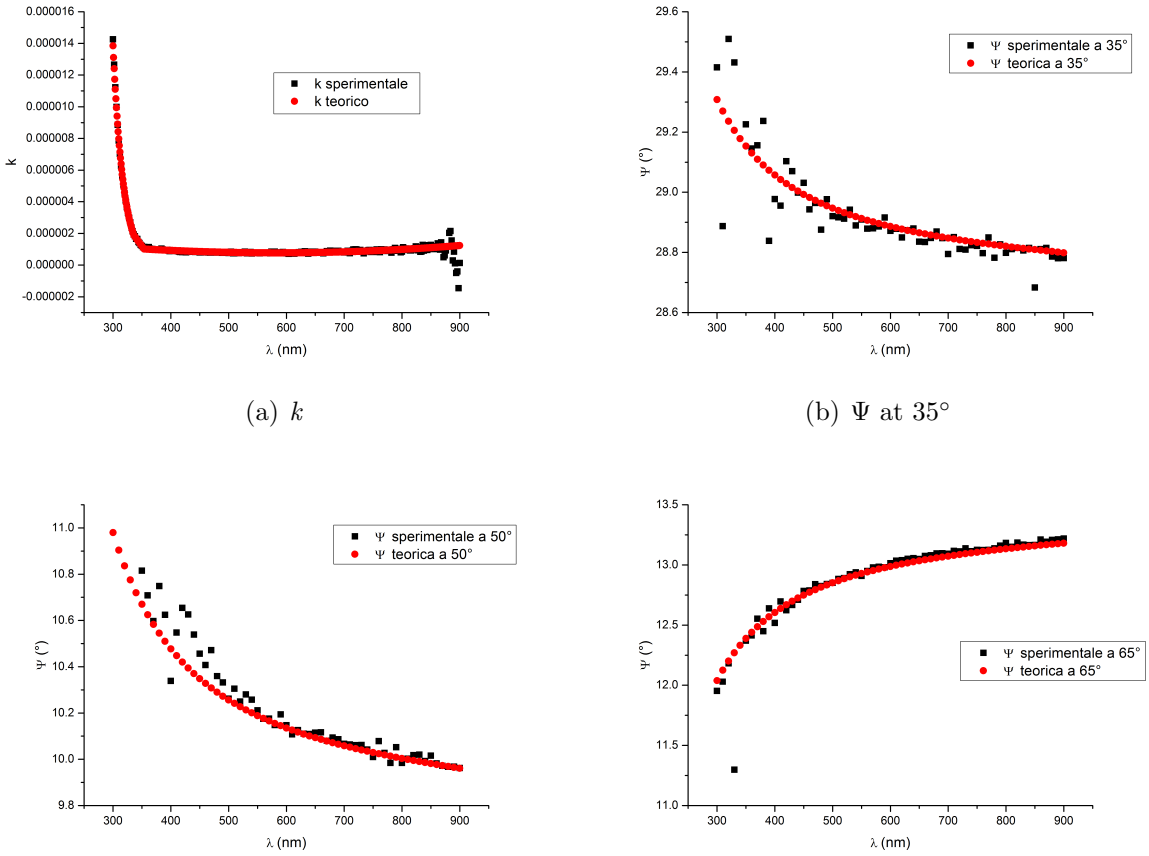

(a) k

(b) Ψ at 35°

(c) Ψ at 50°

(d) Ψ at 65°

Figure 4.1: Experimental points and theorical interpolation for BK7

4.1.2 Sapphire

We used the same model of Soda-lime with $n_{Sapphire}$ given by its specific *Sellmeier* formula:

$$n_{Sapphire}(\lambda) = \sqrt{1 + \frac{1.023789\lambda^2}{\lambda^2 - 0.06144821^2} + \frac{1.058264\lambda^2}{\lambda^2 - 0.1106997^2} + \frac{5.280792\lambda^2}{\lambda^2 - 17.92656^2}} \tag{4.3}$$

We did not consider k as it is almost 0 when 300nm $\leq \lambda \leq$ 900nm at room temperature [18]. Thus, we put $n_{Sapphire}(\lambda) = n^{Sellmeier}_{Sapphire}(\lambda) + c_\alpha$ and varing again c_α we obtained the results shown in the next table:

c_{50}	-0.005
c_{65}	0
c_{80}	-0.011

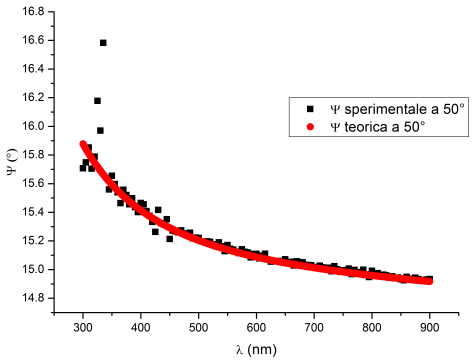

(a) Ψ at 50°

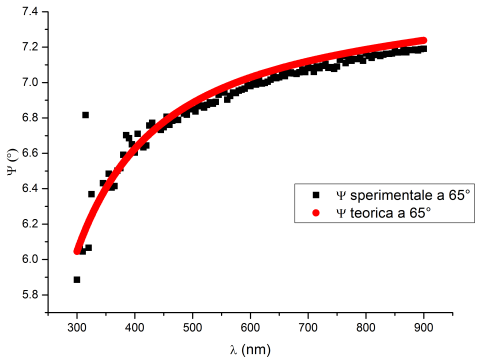

(b) Ψ at 65°

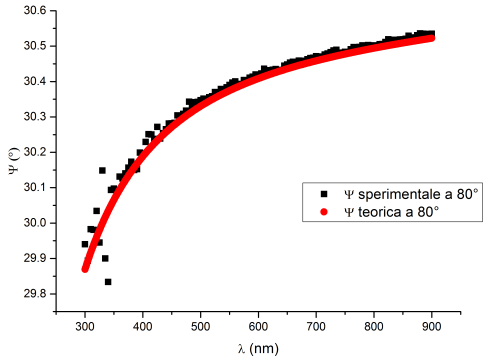

(c) Ψ at 80°

Figure 4.2: Experimental points and theorical interpolation for soda-lime

4.2 Measurements

We performed ellipsometry measurements on all samples of MoS_2 and WS_2, obtaining experimental data of Ψ and Δ at incident angle θ being 35°, 50°, 65° and 80°. We also did reflectance measurements on MoS_2 sample 2 at θ= 50°, 80°. In the next sections we are showing the experimental data.

4.2.1 MoS_2

We present the experimental data obtained in picture 4.3.

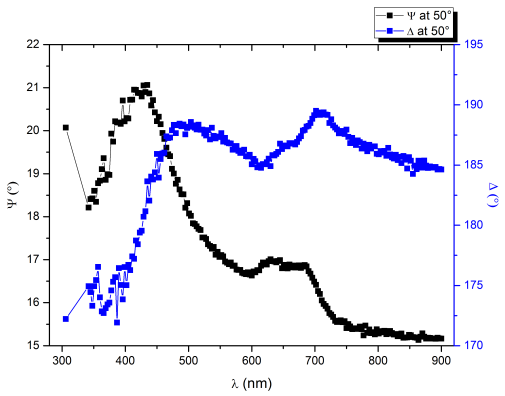

(a) Sample 1 at 50°

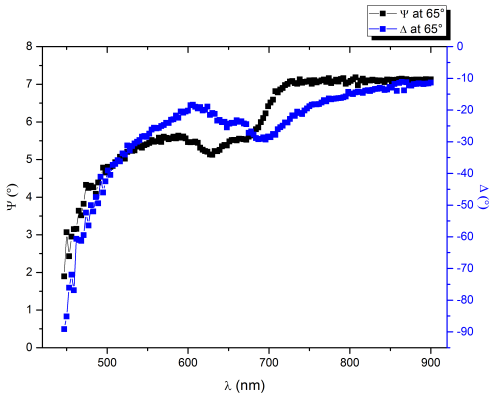

(b) Sample 1 at 65°

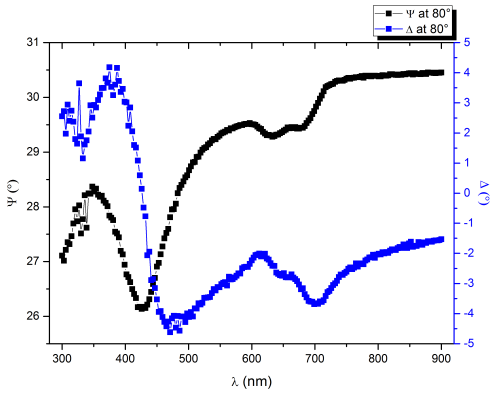

(c) Sample 1 at 80°

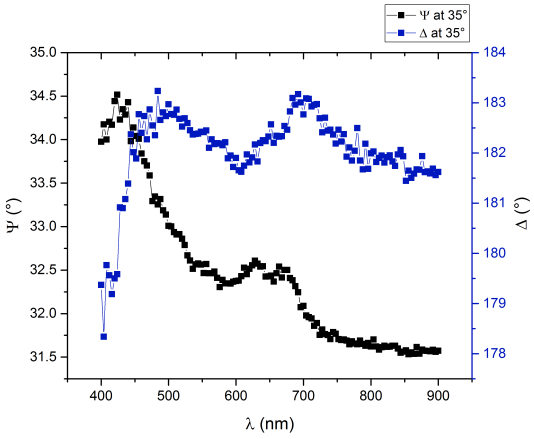

(d) Sample 2 at 35°

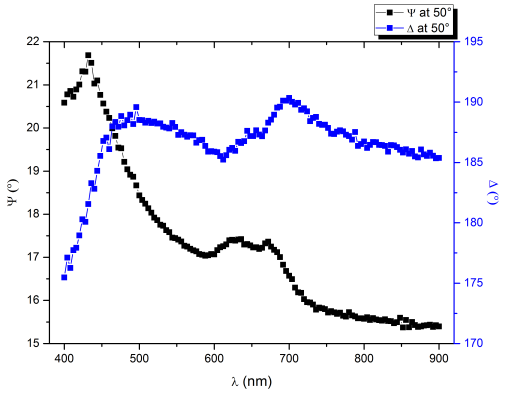

(e) Sample 2 at 50°

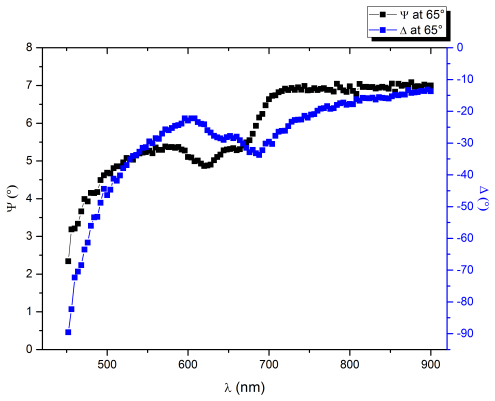

(f) Sample 2 at 65°

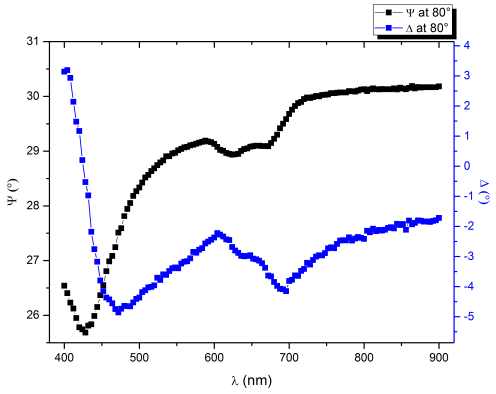

(g) Sample 2 at 80°

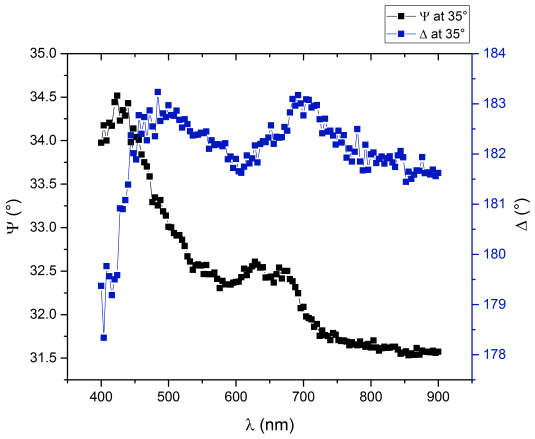

(h) Sample 3 at 35°

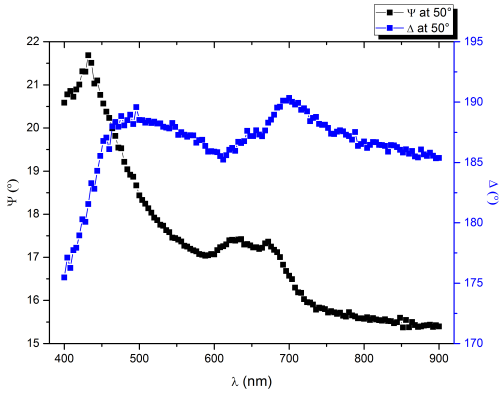

(i) Sample 3 at 50°

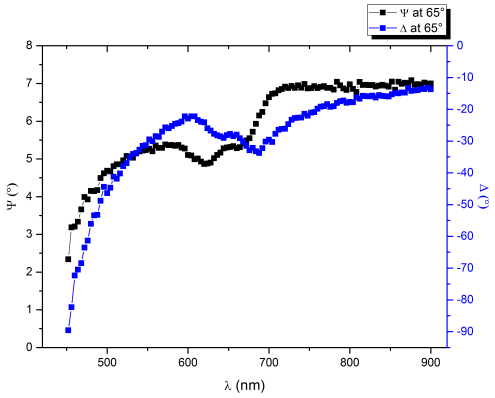

(j) Sample 3 at 65°

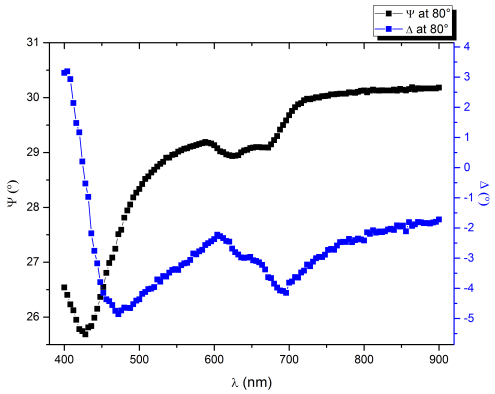

(k) Sample 3 at 80°

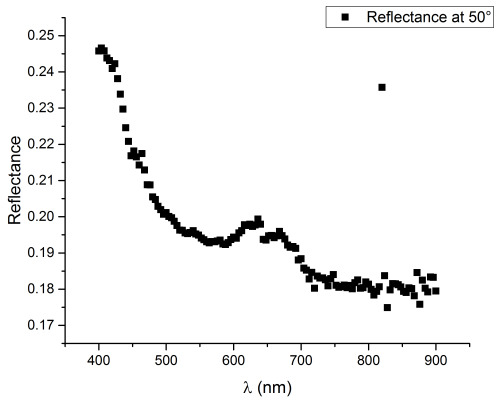

(l) Reflectance of sample 2 at 50°

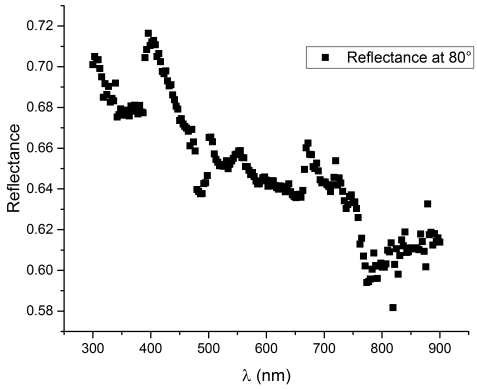

(m) Reflectance of sample 2 at 80°

Figure 4.3: MoS_2 data measured

4.2.2 WS_2

We present the experimental data obtained in picture 4.4.

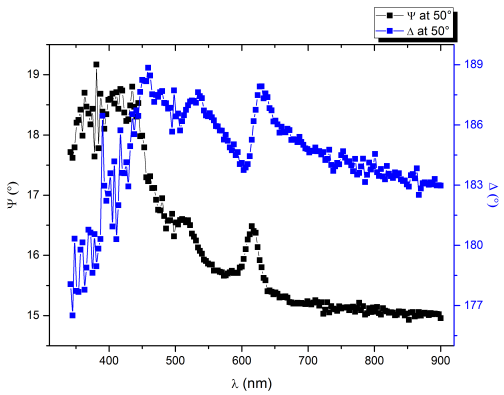

(a) Sample 1 at 50°

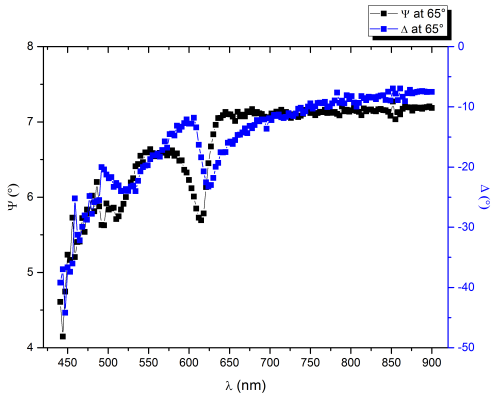

(b) Sample 1 at 65°

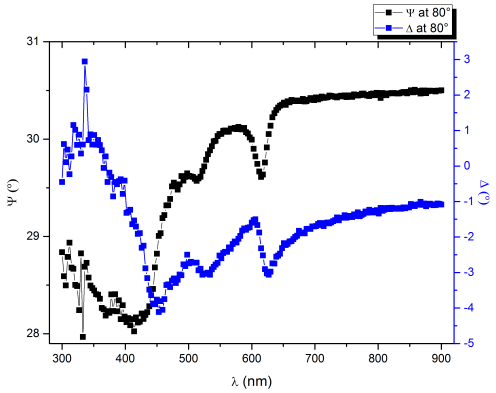

(c) Sample 1 at 80°

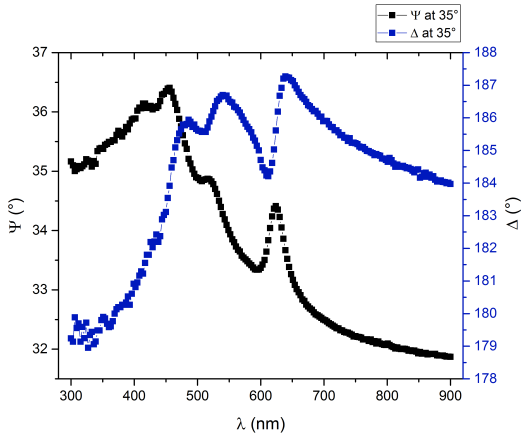

(d) Sample 2 at 35°

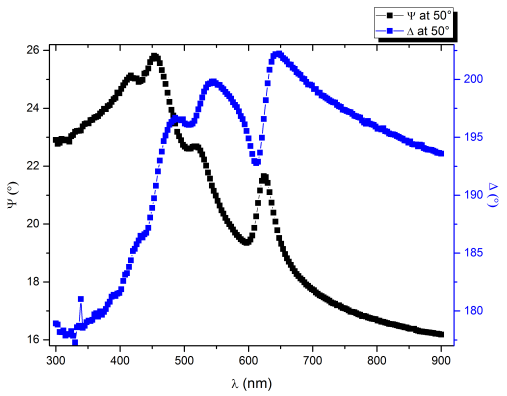

(e) Sample 2 at 50°

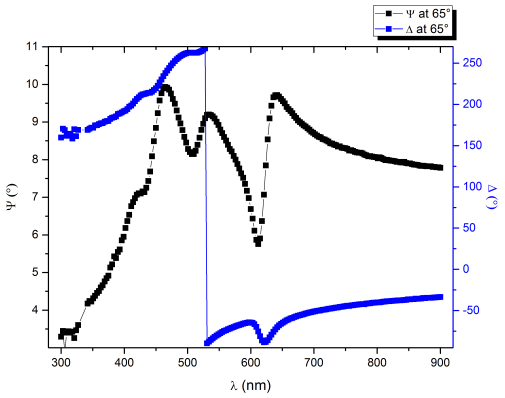

(f) Sample 2 at 65°

Figure 4.4: WS_2 data measured

4.3 Data analysis and controntation with literature

We first applied the Surface Current model using equations 2.25 and implemented it in the Mathematica notebook reported in section 6.1, using the algorithm `FindRoot`. In this way we obtained our values of χ and σ from experimental data, all of them showed in the next graphs. Right after, for MoS_2 sample 2, we used χ and σ extracted to calculate the reflectance theorical value, and confrontated it with the experimental one. We then obtained the values of χ and σ from ε_1 and ε_2 using equations 2.14 and 2.18 of the slab model, implementing this in the Mathematica notebook in section 6.2. Later, we prepared simultaneous plots to confrontate the results of the two different models, assuming the thicknesses $d_{MoS_2} = 6.15$ Å and $d_{WS_2} = 6.18$ Å [15]. At last, we confrontated our results of σ with the analougous results available in [15].

4.3.1 MoS_2

We present our results in pictures 4.5, 4.6 and 4.7.

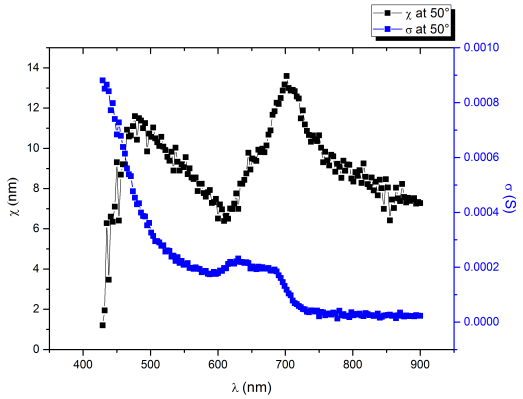

(a) Sample 1 at 50°

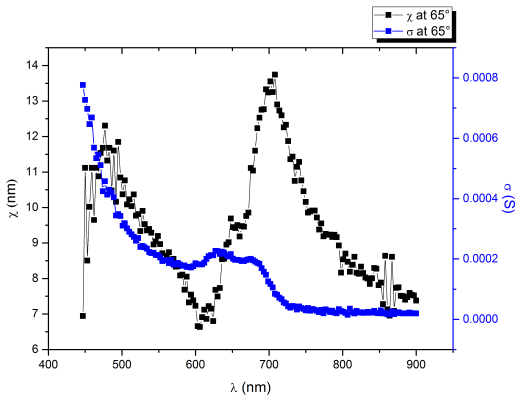

(b) Sample 1 at 65°

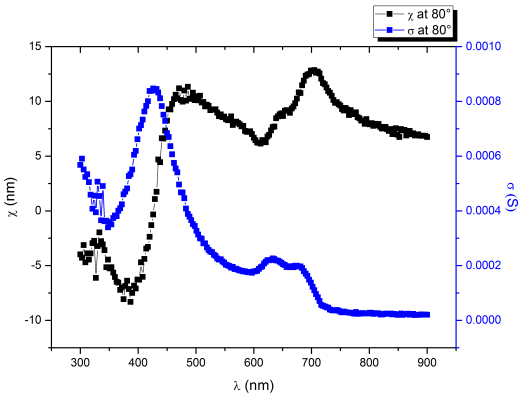

(c) Sample 1 at 80°

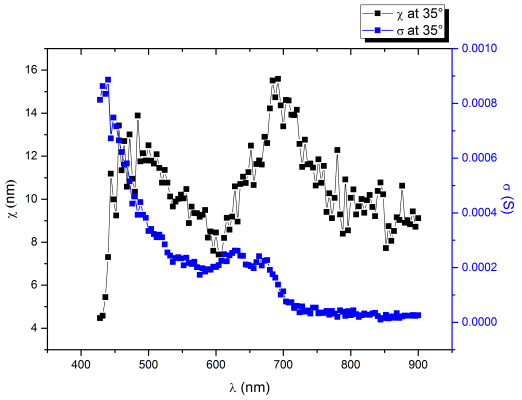

(d) Sample 2 at 35°

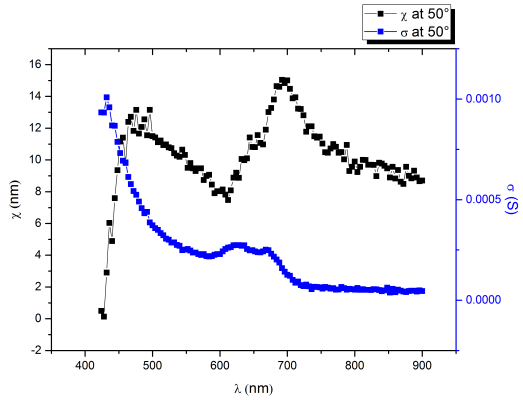

(e) Sample 2 at 50°

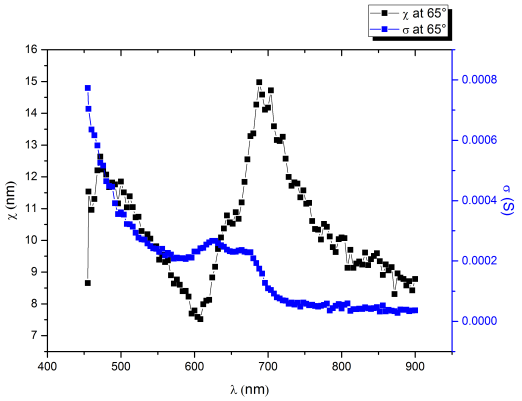

(f) Sample 2 at 65°

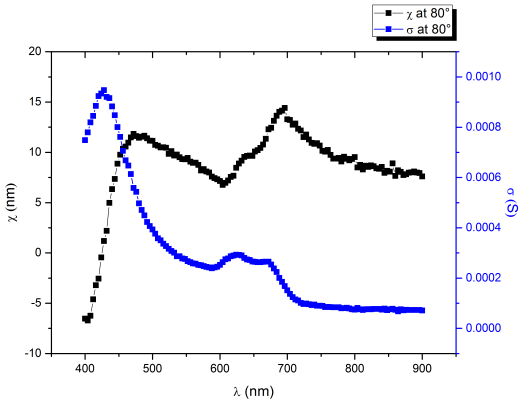

(g) Sample 2 at 80°

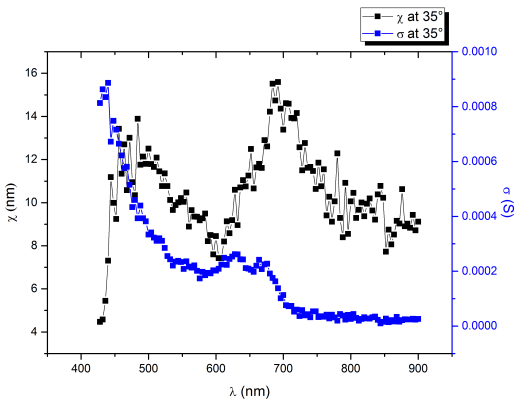

(h) Sample 3 at 35°

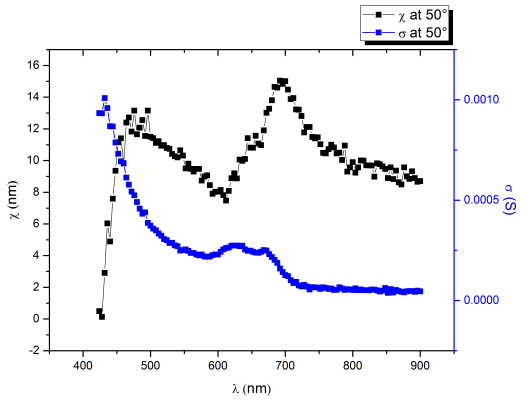

(i) Sample 3 at 50°

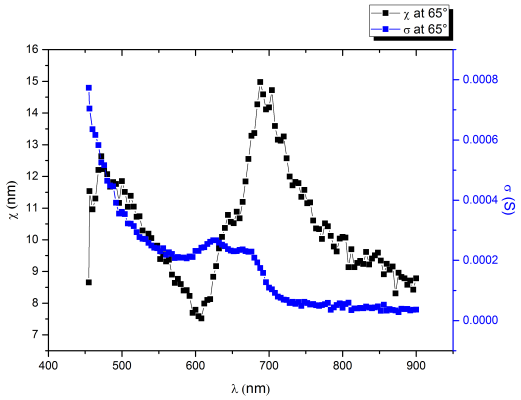

(j) Sample 3 at 65°

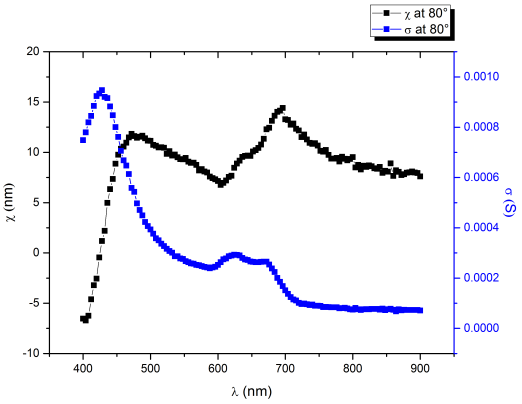

(k) Sample 3 at 80°

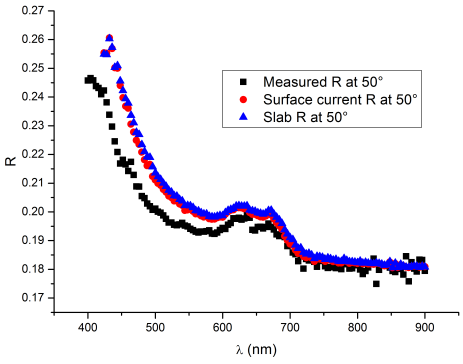

(l) Reflectance of sample 2 at 50°

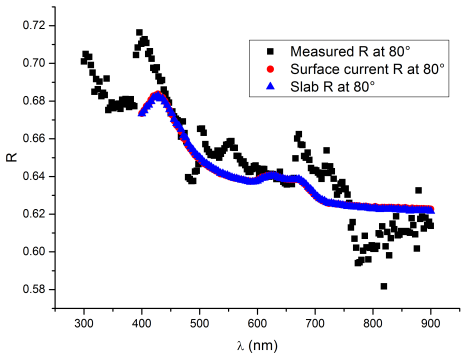

(m) Reflectance of sample 2 at 80°

Figure 4.5: MoS_2 data extracted

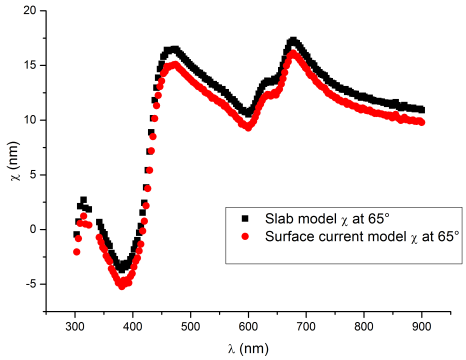

(a) Confrontation of χ

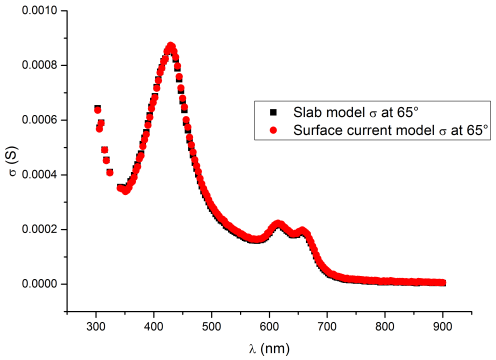

(b) Confrontation of σ

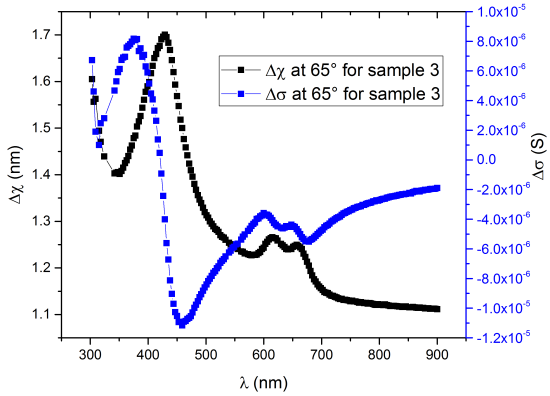

(c) Difference between the two models $\Delta\chi$ and $\Delta\sigma$

Figure 4.6: Confrontation of slab and surface current model for Sample 3 of MoS_2 at 65°

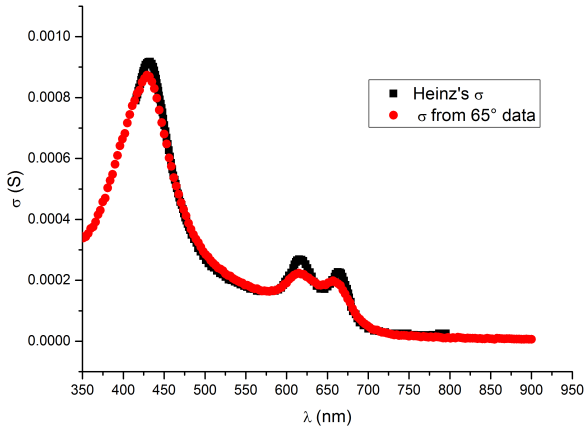

Figure 4.7: Simultaneous plot of σ from surface current model and [15] for MoS_2 sample 3

4.3.2 WS_2

We present our results in pictures 4.8, 4.9 and 4.10.

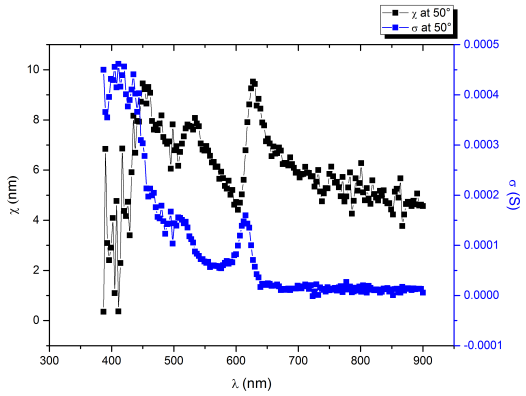

(a) Sample 1 at 50°

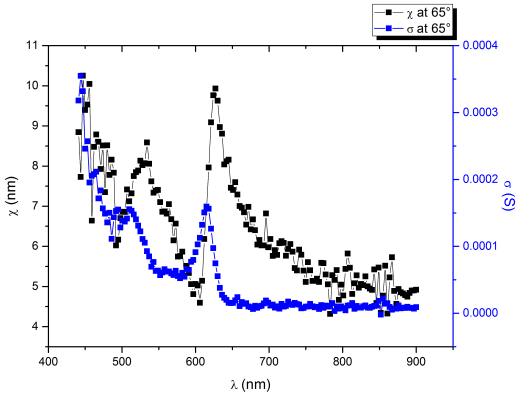

(b) Sample 1 at 65°

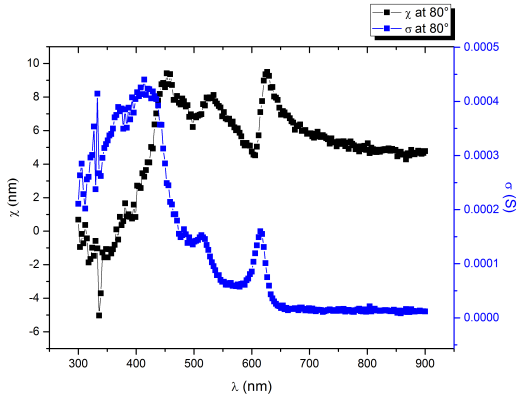

(c) Sample 1 at 80°

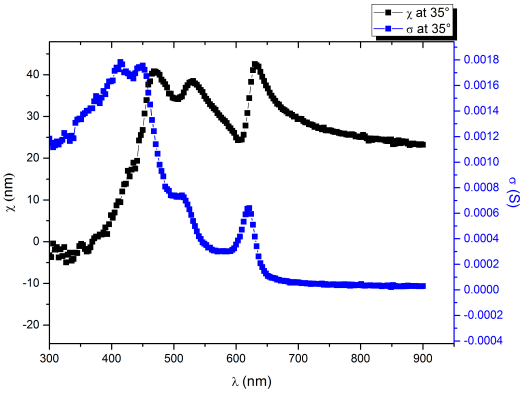

(d) Sample 2 at 35°

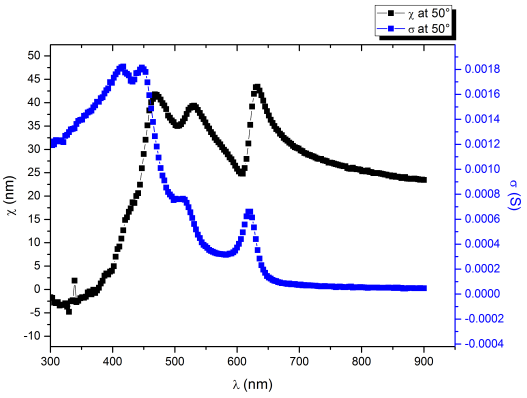

(e) Sample 2 at 50°

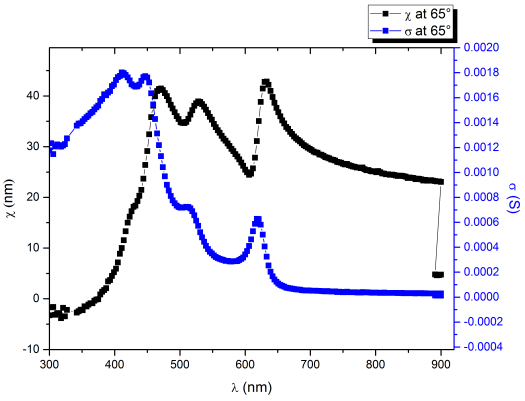

(f) Sample 2 at 65°

Figure 4.8: WS_2 data extracted

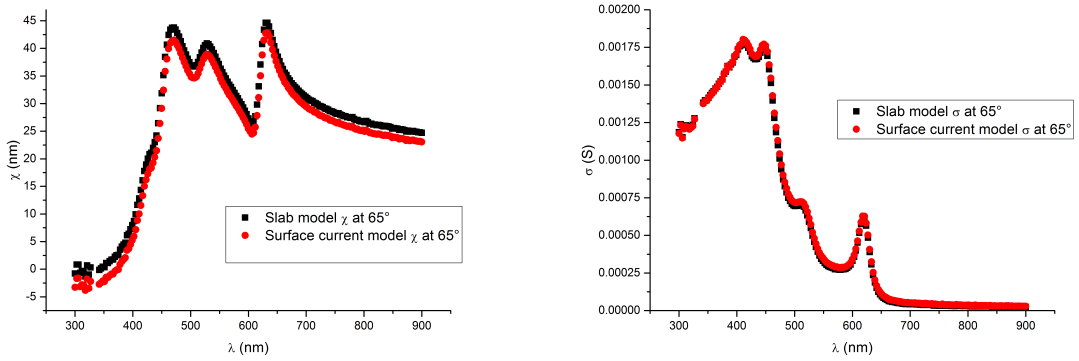

(a) Confrontation of χ

(b) Confrontation of σ

Figure 4.9: Confrontation of slab and surface current model for Sample 2 of WS_2 at 65°

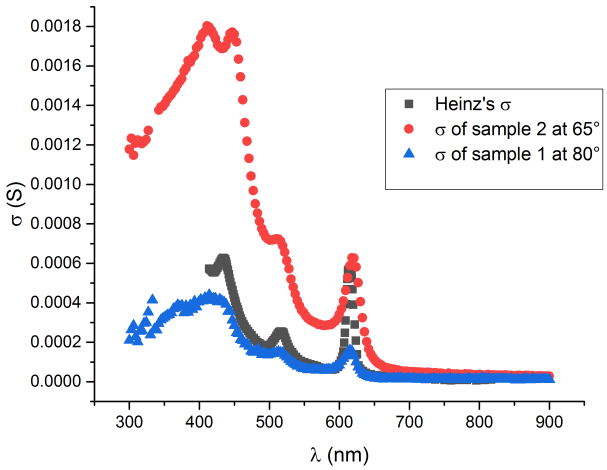

Figure 4.10: Simultaneous plot of σ from surface currentn model and [15] for WS_2

4.4 Discussion

We have succesfully derived χ and σ using the surface current model, appling equations 2.25 and showing the results in pictures 4.5 and 4.8. From the confrontation between the two models shown in pictures 4.6 and 4.9 a difference in both the σ and χ computation arises. As for χ, the difference $\Delta\chi_{MoS_2} \approx 1.3$ nm and $\Delta\chi_{WS_2} \approx 2$ nm is significant. However, these values are a mean as, for both materials, the $\Delta\chi$ distribution follows exactly the σ distribution. This suggests a contribution of ε_2 in χ computiation through equation 2.18. The same is true for $\Delta\sigma$ and, even if the difference $\Delta\sigma$ is much lower, it is still detectable by the measurement and it is much greater than the esperimental error because the $\Delta\sigma$ distribution follows precisly the path of χ and it is not random. The significant χ overstimation by the slab model and the slight difference of σ computation show that the two models are not equivalent and that equations 2.18 are wrong. We then stress the slab model dependance on three parameters (h, ε_1 and ε_2 or, equally, $h, \mathrm{Re}(n_2)$ and $\mathrm{Im}(n_2)$) compared with the surface current model dependance on only two parameters (χ and σ). Moreover, the monolayer thickness h_{MoS_2} or h_{WS_2}, which is a slab model parameter, may change between different structural models used,

between molecule's parts (hard core radius, s or p orbitals) and between different literature sources. The confrontations with the data available in [15] plotted in pictures 4.7 and 4.10 show a difference in the samples quality between MoS_2 and WS_2. The samples 1 and 2 of MoS_2, which have not been plotted, follow Heinz's sample's walk but have significantly disturbed values and are flat at 600 nm $< \lambda <$ 670nm. These facts stress their low quality. On the other hand, sample 3 bears a good accord with Heinz's data and a less fluctuating shape, demostrating its higher quality: in fact, this is our best sample. Instead, WS_2 samples both do not follow Heinz's σ. Interestingly, sample 1 has a good accord with Heinz's data but doesn't present the high peak at $\lambda \approx 610$ nm, while sample 2 has the mentioned peak but it is much higher than Heinz's σ at lower λ. This difference could mean that, while sample 1 is simply of low quality like samples 1 and 2 of MoS_2, sample 2 may be a three layer sample, as its σ values are roughly three times Heinz's ones.
At last, the reflectance measures of MoS_2 sample 2 shown in picture 4.5 (l – m) highlight a poor accord at $\theta = 50°$, where both models slightly overstimate the experimental points, and are unreadable at $\theta = 80°$. Both these facts can be caused by the sample's low quality.

Chapter 5

Conclusions

Because of the facts marked in the previous section, that are the significant $\Delta\chi$, the small but detectable $\Delta\sigma$, and the three-parameter rather than two-parameter dependance, we conclude that the surface current model is not equivalent to the slab model. We have also shown how to correctly derive χ and σ using the surface current model. Finally, we highlight that while the slab model is a three dimensional model adapted to 2D materials, the surface current model is a model specific for a 2D material physical system.

Chapter 6

Appendix A: Mathematica notebooks

6.1 Computation of χ and σ from Ψ and Δ using Surface Current model

```
data = Import["infile.dat", "Table"] (*Expects file with 3 columns:  lambda
in nm, Psi and Delta in degrees.  Substitiute with actual file and path.*)
dim = Dimensions[data] (*column dimension to control the For loop below *)
solutions = (*Solution matrix*)

chi = 1.67 10^(-3)
sigma = 2.627 10^(-5) (*Realistic initial values for FindRoot*)
n1 = 1.0002772 (*Air refractive index*)
n2gen[lam_] := Sqrt[1 + 1.03961212 lam^2 /(lam^2 - 0.00600069867) + 0.231792344
lam^2 /(lam^2 - 0.0200179144) + 1.01046945 lam^2 /(lam^2 - 103.560653)] (*Glass
refractive index*)

(*n2gen[lam_] := Sqrt[1 + 1.023789 lam^2 /(lam^2 - 0.06144821^2) + 1.058264
lam^2 /(lam^2 - 0.1106997^2) + 5.280792 lam^2 /(lam^2 - 17.92656^2)] (*Sapphire
refractive index.  Comment the one you don't need.  Remember that here lambda
is in micrometers, um*) *)

ci = Cos[35 Pi/180] (*Incident angle's cosine.  Put the one you need.*)
ctgen[lam_] := Sqrt[1 + n1^2 (ci^2 - 1)/(n2gen[lam])^2] (*Transmitted angle
cosine*)
eta = 376.7303135 (*Void impendance*)
For[i = 1, i <= dim[[1]], i++,
l = data[[i, 1]]*10^-3; (*Changing lambda in micrometers to n2gen function*)
k = 2 Pi/l; (*k definition in um^(-1)*)
n2 = n2gen[l] - 0.012; (*Put here the right corrective addendum*)
ct = ctgen[l];
Rs[x_, s_] := (n1 ci - n2 ct - I k x - s eta)/(n1 ci + n2 ct + I k x + s eta);
Rp [x_, s_] := (n2 ci - n1 ct + (I k x + s eta) ci ct)/(n2 ci + n1 ct + (I
k x + s eta) ci ct); (*Definitions of reflectivity.  It's possible put it
outside the loop.*)

If[data[[i, 3]] < 180, phase = 0, phase = 360]; (*Definition of phase to correct
```

```
experimental Delta, and set it -180 < Delta < 180*)
sol = x, s /.  FindRoot[180/Pi*ArcTan[ Abs[ Rp[x, s] /Rs[x, s]]] == data[[i,
2]], 180/Pi*Arg[ Rp[x, s] /Rs[x, s]] + phase == data[[i, 3]], x, chi, s, sigma
]; (*Solution algorithm*)
chi = sol[[1]]; (*Resetting initial condition*)
sigma = sol[[2]];
sol = Insert[sol, l*10^3, 1 ];
solutions = Append[solutions, sol]
]
Print[solutions]
Export["outfile.dat", solutions] (*Solution exportation*)
```

6.2 Computation of χ and σ from Ψ and Δ using Slab model

```
data = Import["infile.dat", "Table"] (*Expects file with 3 columns:  lambda
in nm, Psi and Delta in degrees.  Substitiute with actual file and path.*)
dim = Dimensions[data] (*column dimension to control the For loop below *)
solutions = (*Solution matrix*)

n1 = 1.0002772 (*Air refractive index*) n3gen[lam_] := Sqrt[1 + 1.03961212
lam^2/(lam^2 - 0.00600069867) + 0.231792344 lam^2/(lam^2 - 0.0200179144) +
1.01046945 lam^2/(lam^2 - 103.560653)] (*Glass refractive index*)

(*n3gen[lam_]:=Sqrt[1 + 1.023789 lam^2 /(lam^2 - 0.06144821^2) + 1.058264 lam^2
/(lam^2 - 0.1106997^2) + 5.280792 lam^2/(lam^2-17.92656^2)] (*Sapphire
refractive index.  Comment the one you don't need.  Remember that here lambda
is in micrometers, um*) *)

h = 6.18 (*WS2 thickness in Angstrom*)
(*h = 6.15 (*MoS2 thickness in Angstrom, comment the one you don't need*)
*)
c = 299792458 (*Speed of light in m/s*)
e0 = 8.854188*10^(-12)(*Vacuum permittivity in IS units*)
c1 = Cos[80 Pi/180] (*Incident angle's cosine.  Put the one you need.*)
i1 = 15
i2 = 15 (*Realistic initial values for FindRoot*)
Off[General::stop] (*Disable FindRoot's option to hide any failure next the
third one*)
   For[i = 1, i <= dim[[1]], i++,
l = data[[i, 1]]; (*lambda in nm*)
k = 2 Pi/(10 l); (*k definition in Angstrom^(-1)*)
n3 = n3gen[l 10^-3] - 0.0; (*refractive index of substratum with opportune
corrective addendum*)
n2[eps1_, eps2_] := Sqrt[eps1 - I eps2]; (*MoS2 or WS2 refractive index.
Variables are eps1 and 2*) c2[eps1_, eps2_] := Sqrt[1 + (n1/n2[eps1, eps2])^2
(c1^2 - 1)]; (*Refracted angle cosines*)
c3[eps1_, eps2_] := Sqrt[1 + (n2[eps1, eps2]/n3)^2 (c2[eps1, eps2]^2 - 1)];
```

```
rs12[eps1_, eps2_] := (n1 c1 - n2[eps1, eps2] c2[eps1, eps2])/(n1 c1 + n2[eps1,
eps2] c2[eps1, eps2]); (*Definition of various Fresnel coefficients.  They
could be defined also outside the loop*)
rp12[eps1_, eps2_] := (n2[eps1, eps2] c1 - n1 c2[eps1, eps2])/(n2[eps1, eps2]
c1 + n1 c2[eps1, eps2]);
rs23[eps1_, eps2_] := (n2[eps1, eps2] c2[eps1, eps2] - n3 c3[eps1, eps2])
/(n2[eps1, eps2] c2[eps1, eps2] + n3 c3[eps1, eps2]);
rp23[eps1_, eps2_] := (n3 c2[eps1, eps2] - n2[eps1, eps2] c3[eps1, eps2]) /(n3
c2[eps1, eps2] + n2[eps1, eps2] c3[eps1, eps2]);
beta[eps1_, eps2_] := k h n2[eps1, eps2]; (*Argument of the exponential*)
rp123[eps1_, eps2_] := (rp12[eps1, eps2] + rp23[eps1, eps2] Exp[-2 I beta[eps1,
eps2]])/(1 + rp12[eps1, eps2] rp23[eps1, eps2] Exp[-2 I beta[eps1, eps2]]);
rs123[eps1_, eps2_] := (rs12[eps1, eps2] + rs23[eps1, eps2] Exp[-2 I beta[eps1,
eps2]])/(1 + rs12[eps1, eps2] rs23[eps1, eps2] Exp[-2 I beta[eps1, eps2]]);
If[data[[i,3]] < 180, fase=0, fase=360]; (*Definition of phase to correct
experimental Delta, and set it -180 < Delta < 180*)
sol = eps1, eps2 /.  FindRoot[180/Pi*ArcTan[Abs[rp123[eps1, eps2]/rs123[eps1,
eps2]]] == data[[i, 2]], 180/Pi*Arg[rp123[eps1, eps2]/rs123[eps1, eps2]] +
phase == data[[i, 3]], eps1, i1, eps2, i2]; (*Solution algorithm*)
i1 = sol[[1]]; (*Resetting initial condition*)
i2 = sol[[2]];
chi = (sol[[1]] - 1)*h*10^-4; (*calcolation of chi in um*)
sigma = 2 Pi c e0 sol[[2]] h/(l*10); (*calcolation of sigma in Siemens*)
sol = Insert[sol, data[[i, 3]] ,1];
sol = Insert[sol, data[[i, 2]], 1];
sol = Insert[sol, l, 1 ];
sol = Insert[sol, chi, 6];
sol = Insert[sol, sigma, 7];
solutions = Append[solutions, sol]
]
Print[solutions]
Export["outfile.dat", solutions] (*Solution exportation*)
```

Bibliography

[1] Kin Fai Mai, Tony F. Heinz et alia, *Atomically Thin MoS_2: A New Direct-Gap Semiconductor*, September 24th, 2010, Phisical Review Letters.

[2] Wei Li, N. V. Nguyen et alia, *Broadband optical properties of large-area monolayer CVD molybdenum disulfide*, November 21st, 2014, Physical Review.

[3] S. Funke, U. Wurstbauer et alia, *Imaging Spectroscopic Ellipsometry of Mono- and Few-layer*, July 27th, 2016 J. Phys.: Condens. Matter 28 385301

[4] Liu, Lain-Jong et alia, *Optical properties of monolayer transition metal dichalcogenides probed by spectroscopic ellipsometry*, November 18th, 2014, Applied Physics Letters.

[5] Xiao Li, Hongwei Zhu, *Two-dimensional MoS_2: Properties, preparation, and applications*, March 1st, 2015, Journal of Materiomics.

[6] J. Kim, et alia, *Direct exfoliation and dispersion of two-dimensional materials in pure water via temperature control*, September 15th, 2015, Nat. Commun. 6:8294 doi: 10.1038/ncomms9292 (2015).

[7] Xiaolong Liu, Mark C. Hersam et alia, *Rotationally Commensurate Growth of MoS_2 on Epitaxial Graphene*

[8] Chunxiao Cong, Ting Yu et alia, *Synthesis and optical properties of large-scale single-crystalline two-dimensional semiconductor WS_2 monolayer from chemical vapor deposition*, February, 2014, Advanced Optical Materials.

[9] A. Castellanos-Gomez, G. A. Steele et alia, *Laser-thinning of MoS_2: on demand generation of single-layer semiconductor*, May 29th, 2012, Nano Letters.

[10] Xin Liu, Qihua Xiong et alia, *Layer-by-layer thinning of MoS_2 by thermal annealing*, July 2nd, 2013, Nanoscale, 2013, 5, 8904.

[11] V. G. Kravets, A. K. Geim et alia, *Spectroscopic ellipsometry of graphene and excion-shifted van Hove peak in absorption*, April 6th, 2010, Physical Review B.

[12] J. W. Weber, V. E. Colorado and M. C. M. van de Sanden, *Optical constants of graphene measured by spectroscopic ellipsometry*, August 31st, 2010, American Institute of Physics.

[13] Michele Merano, *The wave impedance of an atomically thin crystal*, December 15th, 2015, Optical Society of America.

[14] Michele Merano, *Fresnel coefficients of a two-dimensional atomic crystal*, January 19th, 2016, Physical Review A.

[15] Yilei Li, Tony F. Heinz et alia, *Measurement of the optical dielectric function of monolayer transition-metal dichalcogenides: MoS_2, $MoSe_2$, WS_2, and WSe_2*, November 17th, 2014, Physical Review.

[16] Max Born and Emil Wolf, *Principles of optics*, 2003, Cambridge University Press.

[17] Horland G. Tompkins, *A User's Guide to Ellipsometry*, 1993, Academic Press.

[18] https://refractiveindex.info, visited in 09/07/2017.